2023 IEEE International Conference on Robotics and Automation (ICRA 2023)
May 29 - June 2, 2023. London, UK

A Tactile Feedback Insertion Strategy for Peg-in-Hole Tasks

Oliver Gibbons, Alessandro Albini* and Perla Maiolino

***Abstract*— The Peg-In-Hole (PiH) task performed under uncertain conditions still represents a challenge for autonomous robots. When the peg is not rigidly connected to the robot end-effector, the external forces generated by peg-environment interactions can change the in-hand pose of the peg. This aspect must be taken into account when performing the insertion.**

This paper deals with this problem and proposes an insertion strategy driven by tactile feedback. In particular, we consider holding the peg using a parallel gripper equipped with tactile sensors, whose measurements are processed to capture in-hand rotations of the peg pose. This information is fed back to the robot controller and used to compensate for changes in the peg orientation and end-point position occurring during the task execution. The approach is validated on a real robot using a two-finger gripper equipped with two capacitive-based tactile sensor arrays hosting 20 tactile elements each. We show that the proposed method achieves an insertion success rate of 38/40 with a 0.1 mm clearance between the peg and hole.

I. Introduction

Assembly operations account for a significant portion of the time and cost of an entire production cycle. In particular, 40% of these operations, such as drilling and bolt insertion, can resemble a Peg-In-Hole (PiH) task [1], [2]. Therefore, autonomous strategies to solve the PiH problem have been extensively researched for decades by the robotics community [3]. Although this task can be considered solved when the geometry and the pose of both peg and hole are known, those strategies cannot be used in fast production lines because it is not feasible to re-calibrate or change the whole setup due to time constraints [4]. One possibility to avoid long setup times consists of assuming that the centre of the hole is known with uncertainty (e.g. detected with a camera) and letting the robot perform the insertion under these conditions.

For this reason, several solutions have been proposed to address the PiH task starting from an initial estimation of the centre of the hole and using sensors to perform the insertion. One common approach is to process the measurements of F/T sensors mounted on the robot wrist [5]–[10]. These are used to sense the forces generated by the peg-hole interactions and drive the robot to precisely find the centre of the hole. However, F/T sensors increase the cost of the overall system and require a high control frequency. Therefore, different approaches attempt to perform the PiH task through retrieving the position of the hole by performing an analysis of the contact state, exploiting sensors at the robot joints

All the authors are with the Oxford Robotics Institute (ORI), University of Oxford, UK.
*Corresponding author e-mail: alessandro@oxfordrobotics.institute
We gratefully acknowledge support by EPSRC Programme Grant 'From Sensing to Collaboration' (EP/V000748/1)

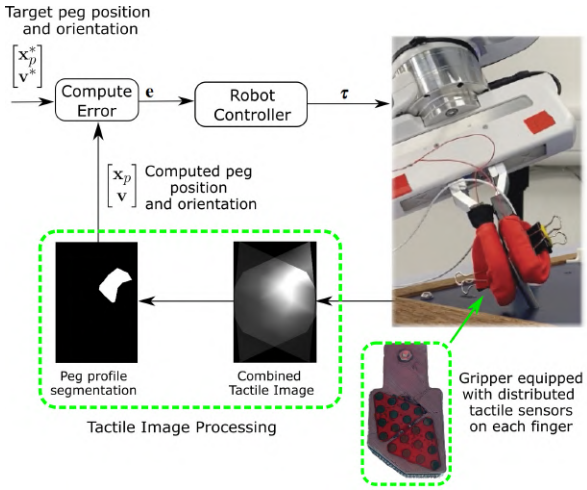

Fig. 1. Overview of the approach. The robot is performing the insertion of a cylindrical peg held by a parallel gripper equipped with capacitive-based tactile sensors on each finger. The tactile measurements are processed to extract the current position and the in-hand orientation of the peg $\mathbf{x_p}$ and $\mathbf{v}$. These are fed back to an impedance controller which follows the two references $\mathbf{x_p^*}$ and $\mathbf{v}^*$.

[11]–[13]. These methods can be applied for a specific peg geometry and are usually coupled with compliant control strategies to compensate for inaccuracies in the estimation of the hole centre.

The previously described approaches assume the peg to be rigidly attached to the robot end-effector. The advantage is that there is then no uncertainty in the in-hand pose of the peg when its geometry is known. However, this represents a limitation in assembly tasks where other operations besides the PiH must be performed, since the end-effector would then have to be replaced. In this scenario, a single gripper used to perform multiple operations would be more suitable. However, in these conditions the complexity of the task increases as external forces due to peg-environment interactions can change the peg pose.

Examples of works considering the peg held by a gripper or a dexterous hand can be found in [14], [15]. However, they do not consider the problem of detecting and compensating for large variations in the in-hand peg pose. In particular, in [14] different pegs are manipulated by a parallel gripper equipped with high-resolution tactile sensors. Due to the friction provided by the compliant layer of the sensor and the large width of the peg (providing a large contact area), they can ensure a stable grasp. A different approach is presented in [15], which addresses the problem of inserting a cylindrical peg using a compliant-controlled robot hand.

Here, the peg is grasped with three fingers. The controller regulates the force measurements gathered from the load cells (embedded in the fingertips) to ensure a stable grasp. The compliance of the hand allows for variations of the peg in-hand pose, however, in this case, the peg movement was not directly detected or compensated for. The insertion strategy consists of a sequence of open-loop fixed robot motions. The transition between each motion is based on the evaluation of the resultant contact forces sensed with load cells.

To summarize approaches proposed in the literature address the PiH task by considering none or small variations of the peg in-hand pose. The majority assumes the peg is rigidly attached to the robot end-effector. However, when the peg is free to move, the techniques based on the analysis of the contact state cannot be directly applied without a method to estimate the in-hand peg pose. Similarly, F/T sensors integrated into the wrist cannot be used to precisely measure the contact forces acting on a movable peg. In this respect, tactile sensing has already been proven to be effective to retrieve the in-hand pose of an object [16], [17] or to localize contacts [18], [19].

In this paper, we consider the scenario where the in-hand peg pose can change due to contact forces and we present a strategy to address the PiH task by exploiting tactile feedback. Tactile sensors, integrated on a parallel gripper, are used to compute the in-hand orientation of the peg and the position of its end-point. Similarly to other methods, the robot starts with an initial estimate of the position of the hole centre. Then an exploration of the area of interest is performed. Tactile measurements are used in this phase to track the end-point of the peg, ensuring that it is following the desired trajectory and detecting the presence of the hole. Once found, the insertion strategy consists of aligning the peg with the plane containing the hole. In this phase, tactile information is fed back to the closed-loop controller to compensate for possible in-hand motions due to external forces. Figure 1 shows an overview of the insertion strategy.

The rest of the paper is organised as follows. Section II contains a formal description of the problem and the assumptions which have been made. Section III describes how tactile sensing measurements are used to retrieve the in-hand orientation of the peg. The search and insertion strategies are explained in Sections IV and V respectively. The experimental setup we used to validate the approach is described in Section VI. Results are presented and discussed in Section VII. The conclusion follows.

II. Problem Description

This paper considers the problem of inserting a cylindrical and chamferless peg of known diameter d in a hole of diameter D, using a robot arm. The values d and D are chosen following the rationale described in [15], where a dimensionless clearance value is defined as $c = (D-d)/D$. As reported in [15], $c = 0.02$ defines a sufficiently difficult insertion task where the clearance is small enough to influence the insertion time of an assembly task when performed by human operators. The hole lies on a planar surface and its location $\mathbf{x}_h \in \Re^3$ is assumed to be known with uncertainty in the interval $[\mathbf{x}_h - \mathbf{\Delta}_x, \mathbf{x}_h + \mathbf{\Delta}_x]$, where $\mathbf{\Delta}_x \in \Re^3$.

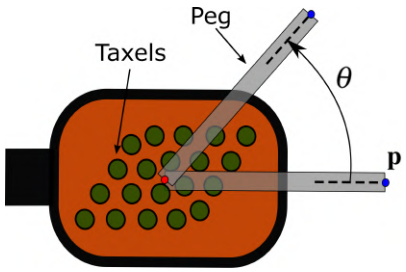

Fig. 2. Sketch representing the peg held by the gripper. We do not consider translations of the peg along the plane but we assume that external forces have the effect of changing the in-plane orientation of the peg, making it pivot around the center of the finger.

The peg of length L is placed in a known location and grasped using a robot equipped with a two-finger parallel gripper. Tactile sensors are available on both fingers and are used to detect the effect of external forces acting on the peg. In particular, we consider a tactile sensing system composed of a set of transducers, i.e. *taxels*, placed on a rigid flat part and covered with a layer of compliant material. This layer filters the pressure applied on top of the sensor and allows for more stable grasping. Figure 1 shows the capacitive-based tactile sensors which was integrated on both fingers.

Since the peg is not rigidly attached to the robot gripper, peg-hole or peg-environment interactions can change the relative in-hand pose of the peg. In this paper, we assume that external forces will cause the peg to pivot around the centre of the two fingers as shown in Figure 2. We also consider motions on the remaining axes negligible, since we assume that the grasping force and the friction of the compliant layer allow for small changes in the peg's relative position (similarly to [14], [15]). In this context, we use tactile sensing to compute the in-hand peg orientation $\theta \in \Re$ and the position of the end-point $\mathbf{p} \in \Re^3$ (defined in Figure 2 in the local frame of the fingers) at each time instant. This information is fed back to control the robot during the insertion task.

III. Estimating the Peg In-Hand Pose with Tactile Sensors

This Section describes how tactile sensors are exploited to retrieve the peg orientation and its end-point position with respect to the robot base.

It is assumed that the sensing system, embedded in the fingers, generates an array of measurements corresponding to the pressure values sensed by the taxels at a fixed sampling time. When the gripper is holding the peg, the pressure distribution generated by the peg in contact with the fingers is captured by the tactile system. To process tactile measurements, we converted the raw responses of the sensors in two *tactile images*, $\mathbf{I}_L$ and $\mathbf{I}_R$ for the left and right fingers respectively, by following the procedure reported in [20]. As shown in Figure 3, the gripper is holding the peg and

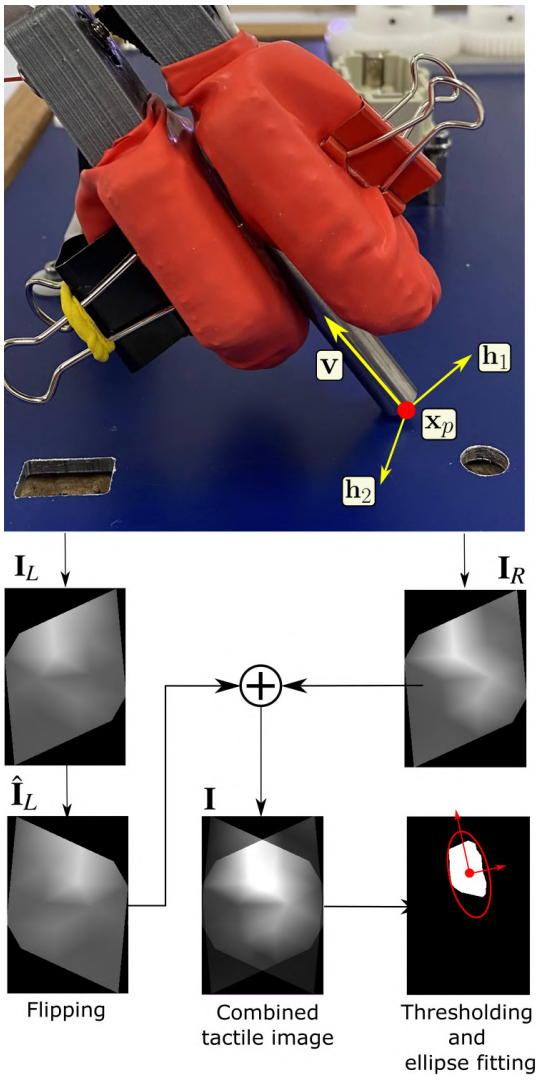

Fig. 3. Processing pipeline executed at each time instant. Two tactile images are generated from the two fingers. The images are combined to better highlight the profile of the peg. The tactile image $\mathbf{I}$ is then processed to extract the in-hand orientation of the peg $\mathbf{v}$ and its end-point position $\mathbf{x}_p$ with respect to the robot base frame.

the corresponding pressure distribution is reconstructed and mapped on the two tactile images. Since the two images encode the geometry of the peg, they can be processed to extract its orientation. However, from Figure 3 it can be noted that the pressure profile is slightly different for the two images. Indeed, the compliance of the soft material covering the fingers allows for very small movements, resulting in an unbalanced pressure distribution between the two fingers. This will lead to inaccuracies when computing the orientation of the peg if only one image is used.

This problem can be addressed by combining the two tactile images. The resulting sensor output is then computed as:

$$\mathbf{I} = \hat{\mathbf{I}}_L \oplus \mathbf{I}_R \tag{1}$$

where $\oplus$ corresponds to the sum of each pixel saturated to fullscale of the image and with $\hat{\mathbf{I}}_L$ we denote the image $\mathbf{I}_L$ flipped with respect to the vertical axis. Figure 3 shows the result of this operation. As visible from the picture, this leads to an image representing a more uniform pressure profile, which better encodes the part of the peg in contact with the fingers. It must be noted that this operation does not require the peg to be symmetric, it just highlights the profile of the object parts which are both in contact with the fingers.

To compute the peg orientation from $\mathbf{I}$ we used the method described in [21]. Firstly, a thresholding operation is performed on $\mathbf{I}$. This allows for the removal of the background and the segmentation of the peg profile. Secondly, the first and second-order image moments are computed to fit an ellipse as shown in Figure 3. The vector directed along the major axis of the ellipse can then be used to compute the angle θ. The end-point position, $\mathbf{x}_p$, can then be calculated using the knowledge of the length L.

Assuming the peg is pivoting as shown in Figure 2, the relative in-hand pose of the peg with respect to the centre of the fingers can be described by the following transformation matrix:

$$\mathbf{T}_p^f = \begin{bmatrix} 1 & \cos\theta & -\sin\theta & L\cos\theta \\ 0 & \sin\theta & \cos\theta & L\sin\theta \\ 0 & 0 & 1 & 0 \\ 0 & 0 & 0 & 1 \end{bmatrix} \tag{2}$$

which can be expressed with respect to the robot base frame as:

$$\mathbf{T}_p^b = \mathbf{T}_f^b \mathbf{T}_p^f = \begin{bmatrix} \mathbf{h}_1 & \mathbf{h}_2 & \mathbf{v} & \mathbf{x}_p \\ 0 & 0 & 0 & 1 \end{bmatrix} \tag{3}$$

where $\mathbf{T}_f^b$ represents the transformation matrix between the robot base and the centre of the fingers. In Equation (3), the three unitary vectors $\mathbf{h}_1$, $\mathbf{h}_2$ and $\mathbf{v} \in \Re^3$ define the frame of the peg in robot base coordinates which is centered in $\mathbf{x}_p \in \Re^3$ corresponding to the end-point position. These quantities are visible at the top of Figure 3 marked with yellow color. In this paper, we do not consider $\mathbf{h}_1$ and $\mathbf{h}_2$, since we assume to control the motion of the end-point $\mathbf{x}_p$ and the orientation vector $\mathbf{v}$. These quantities are computed at each time instant to track the in-hand free motions of the peg occurring while the robot is interacting with the environment.

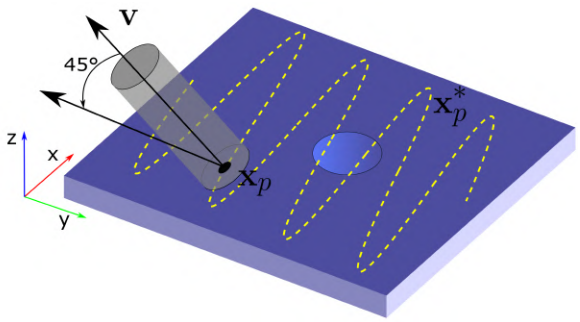

Fig. 4. Exploration strategy used in this paper. The yellow line represents the desired trajectory to be followed with the end-point of the peg. The peg is tilted by 45° with respect to the plane.

IV. Search Strategy and Hole Detection

After grasping the peg from its initial position, the robot approaches the surface where the hole is located. Since the peg position $\mathbf{x}_h$ is known with a certain confidence, the robot picks a random initial position $\mathbf{x}_0 \in [\mathbf{x}_h - \boldsymbol{\Delta}_x, \mathbf{x}_h + \boldsymbol{\Delta}_x]$ to start an exploration procedure. We assume to perfectly know the z component of $\mathbf{x}_h$, therefore, $\Delta_{x,3} = 0$.

We adopted a sinusoidal *spray paint* like motion as an exploration strategy [22]. The desired motion of the robot end-effector is then described by two sinusoidal motions on the plane (one for each axis). Since the hole diameter D is known, the frequencies of the sinusoidal motions can be tuned to ensure the distance between successive points in the path is low enough to ensure the hole is located along the path. The amplitudes can be computed to cover the required search space.

Figure 4 graphically represents the spray paint path $\mathbf{x}_p^*$, which is followed using a Cartesian impedance controller. In particular, to ensure the peg is in contact with the surface, we defined $x_{p,z}^*$ to be slightly lower than the surface height. An offset of 0.01 m was used in this paper. Furthermore, similarly to [15] we kept the peg tilted at 45° during the exploration phase to increase the likelihood of a collision between the edge of the peg and the edge of the hole (see Figure 4). During this phase, tactile sensors are used to update changes to $\mathbf{x}_p$ due to frictional forces between the peg and the surface. In this way, the controller ensures that the desired trajectory $\mathbf{x}_p^*$ is followed by the peg end-point.

The impedance controller that constantly pushes on the surface during the exploration, causes the peg to slide and fall into the hole when passing over it. It must be noted that the peg and hole are not required to be perfectly aligned. The peg will fall into the hole due to: (i) the tilt angle (see Figure 4); (ii) the compliance in the (x,y) plane given by the impedance controller; (iii) the degree of freedom of the peg allowing for the rotation around the pivot point (see Figure 2).

This causes a sudden change in the response measured by the tactile system which can be detected by performing a numerical differentiation on the average sensor responses and comparing it with a threshold value which has been experimentally tuned on the specific tactile sensor we used. Furthermore, during this search phase, the fingers are oriented as shown in Figure 3 (with the back of the finger facing the surface). In this way, we maximise the changes in perpendicular force measured by the sensor.

Once the hole is detected, its position with respect to the robot base frame is defined as $\mathbf{x}_h \cong \mathbf{x}_p$, i.e. it is approximated to be equal to the peg end-point position computed at the time instant corresponding to the detection of the hole. This inaccuracy is handled by keeping the robot compliant during the insertion phase as explained in the next Section.

V. Insertion Phase

As an outcome of the search strategy described in the previous Section, the robot ends up in a configuration similar to that sketched in Figure 5(a), where $\mathbf{v}$ is the vector representing the orientation of the peg with respect to the robot base frame (see Section III).

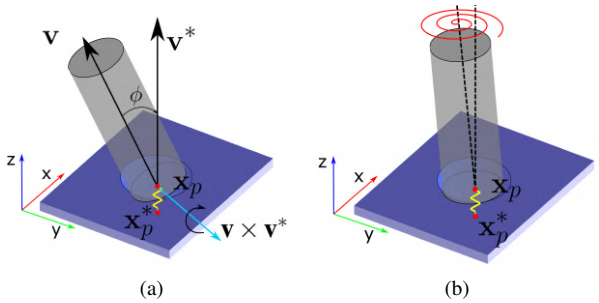

Fig. 5. Graphical representation describing the two steps of the insertion phase. (a) The vector $\mathbf{v}$ representing the orientation of the peg, is aligned with $\mathbf{v}^*$ by minimizing the angle ϕ. This is performed by rotating $\mathbf{v}$ around the vector $\mathbf{v} \times \mathbf{v}^*$ represented by the light blue line. While the peg is rotating, $\mathbf{x}_p$ is pulled toward $\mathbf{x}_p^*$ by the impedance control, simulating a virtual spring along the z-axis. Even if the orientation of the peg can change due to external forces, tactile feedback is used to compute $\mathbf{v}$ and $\mathbf{x}_p$ online. (b) Since the angle ϕ is computed with an error (due to the spatial resolution of the sensing system), a final open-loop phase consisting of a spiral movement is required to complete the insertion.

The insertion strategy proposed in this paper consists of two steps. In the first, the robot is controlled to align the peg with the normal of the plane (see Figure 5(a)). In this phase, $\mathbf{v}$ and $\mathbf{x}_p$ are computed at each time instant and in-hand rotations caused by external forces can be actively compensated for by the controller. In an ideal condition, the first step would be enough, however, tactile sensors allow for the computation of θ with an error. Therefore, an additional open loop adjustment is performed to overcome this inaccuracy.

A. Insertion with Closed-Loop Control

The first phase of the insertion is sketched in Figure 5(a) and consists of rotating the peg to align it with the desired vector $\mathbf{v}^* = [0,0,1]^\intercal$ corresponding to the normal to the plane. Furthermore, during the rotation, we constrain the first two components $\mathbf{x}_p$ to stay fixed at the center of the hole. The target point for the z-axis is then defined below the surface. If this reference is followed with a Cartesian impedance controller, the virtual spring has the effect of pulling the end-point of the peg inside the hole (see Figure 5(a)). Therefore, we redefine the target reference positions as:

$$\mathbf{x}_p^* = \begin{bmatrix} x_{h,x} \\ x_{h,y} \\ x_{p,z}^* \end{bmatrix} \in \Re^3 \tag{4}$$

where $x_{h,x}$ and $x_{h,y}$ are the first two components of $\mathbf{x}_h$ computed as in Section IV, and $x_{p,z}^*$ is a constant reference value defined below the surface, using the same 0.01 m offset used during the search phase. The control error can be then written as:

$$\mathbf{e} = \begin{bmatrix} \mathbf{x}_p - \mathbf{x}_p^* \\ (\mathbf{v} \times \mathbf{v}^*)\,\phi \end{bmatrix} \in \Re^6 \tag{5}$$

where ϕ represents the angle formed by the two vectors $\mathbf{v}$ and $\mathbf{v}^*$ and is computed as $\phi = \cos^{-1}(\mathbf{v} \cdot \mathbf{v}^*)$, since $|\mathbf{v}| = |\mathbf{v}^*| = 1$.

It must be noted that during the insertion operation, although the in-hand peg position can change due to peg-hole interactions, tactile feedback is used to compute $\mathbf{v}$ and $\mathbf{x}_p$ online for use in the control law, which is computed as shown in Equation (6):

$$\boldsymbol{\tau} = \mathbf{J_p}^\top \left(-\mathbf{K}\,\mathbf{e} - \mathbf{K}_I \int \mathbf{e} - \mathbf{D}\mathbf{J_p}\dot{\mathbf{q}} \right) \tag{6}$$

where $\boldsymbol{\tau}$ is the commanded torque, $\mathbf{K}$ and $\mathbf{D}$ are the stiffness and damping matrices respectively, $\mathbf{K}_I$ is a gain matrix, $\dot{\mathbf{q}}$ is the robot joint velocity and $\mathbf{J}_p$ is the Jacobian matrix of the peg end-point expressed with respect to the robot base frame, computed and updated at each time instant using the information on the in-hand peg pose retrieved as in Section III.

Equation (6) corresponds to an impedance controller with an integral term, where $\mathbf{K}_I$ only affects the orientation part of the error. A proportional term alone cannot be sufficient in this scenario. Integral action is necessary to overcome the contact forces generated by peg-hole interactions that prevent the insertion. Furthermore, the integral is saturated to avoid overshoots in the robot motions.

During the insertion phase, the controller modulates the pushing force on the vertical axis depending on the value of ϕ. When ϕ is large it means that the peg is not aligned with the vertical axis and the controller should push with a low force to minimize contact forces that may potentially change the peg's in-hand pose by a large amount. On the contrary, when ϕ decreases, the peg is aligning with $\mathbf{v}^*$. Therefore, the robot can push harder to force the insertion. We achieved this behavior inside the controller by making the stiffness value on the z-axis dependent on ϕ. It is computed as follows:

$$\begin{aligned} [\mathbf{K}]_{3,3} &= K_{max} * \exp(-a\phi) \\ a &= -\tfrac{1}{\phi_0} \ln\left(\tfrac{K_{min}}{K_{max}}\right) \end{aligned} \tag{7}$$

where ϕ_0 is the initial value of ϕ upon peg-hole contact. Therefore, the stiffness on the z-axis smoothly increases from K_{min} to K_{max} as long as ϕ is getting smaller. It must be noted that the initial angle, ϕ_0, does not correspond to the tilt angle kept during the exploration phase. Indeed, it also takes into account the in-hand rotation of the peg that may occur when following the desired spray-paint path (see Section IV).

B. Open-Loop Adjustment

As previously mentioned, the computation of θ (and thus $\mathbf{v}$ and $\mathbf{x}_p$) from tactile sensing measurements is affected by an error. The magnitude of the error depends on the spatial resolution of the tactile sensing system. Therefore, even when $\mathbf{e}$ (see Equation (5)) is close to zero, the peg could not be perfectly aligned with $\mathbf{v}^*$. Due to the small peg-hole clearance, this misalignment can prevent the successful insertion of the peg.

A solution to this problem is to complete the insertion with a final open-loop phase where tactile measurements are not used. The robot is commanded to keep the approximate end point of the peg fixed whilst changing the orientation of the peg in a spiral motion, as shown in Figure 5(b), whilst constantly pushing along the z-axis.

(a) (b) (c)

Fig. 6. Sensorised finger used in this paper. (a) Tactile sensor placement. The fingers contain 20 taxels evenly spaced by 7.5 mm. (b) Compliant layer added on top of the sensors. (c) Rubber cover holding the layers in place.

VI. Experimental Setup

The approach has been tested using a Panda robot arm and the NIST taskboard #1 [23]. The diameters of the peg and hole are $d = 8\,\text{mm}$ and $D = 8.1\,\text{mm}$ respectively. Therefore the dimensionless clearance discussed in Section II is $c = 0.0123$. The length of the peg L is 0.05 m. The original Panda gripper was modified to integrate the tactile sensing system in the fingertips. One of the fingers equipped with tactile sensors is shown in Figure 6. The sensing technology used in this paper is CySkin [24]. Two modules composed of 10 capacitive-based taxels each have been integrated into the fingers. The distance between each nearby taxel is 7.5 mm. Tactile measurements are acquired at 10 Hz and connected to the same acquisition board which guarantees the two modules are synchronized when collecting measurements. The sensors are covered with a conductive ground plane glued with a 1 mm thick elastomer made of Ecoflex 00-20 acting as a mechanical low pass filter. Finally, everything was held in place using a red rubber cover, that provided enough friction to prevent relative translational movement.

The method was tested under the following assumptions: (i) the robot starts the exploration procedure by taking a random point inside a $0.06 \times 0.06\,\text{m}^2$ area containing the hole. Therefore, $\boldsymbol{\Delta}_x = [0.03\,\text{m}, 0.03\,\text{m}, 0]^\top$; (ii) the peg is placed in a rack aligned with the normal at the plane and grasped in the same manner at the beginning of each attempt. (iii) the position of the task board was marked and kept fixed throughout all experiments.

To classify the peg insertion as a success or failure in a repeatable manner, a switch was placed below the hole. This was connected to a micro-controller such that the robot could stop and classify an attempt as a success if the switch was pushed. An attempt was classified as a failure if forcefully stopped by the user to prevent a collision or if the search phase was not completed before a given time of 100 seconds.

VII. Results

The robot attempted to complete 40 peg insertions with the setup described in Section VI. Table I summarises the results. The average completion times and success rates of each stage of the PiH task are given. After 40 attempts,

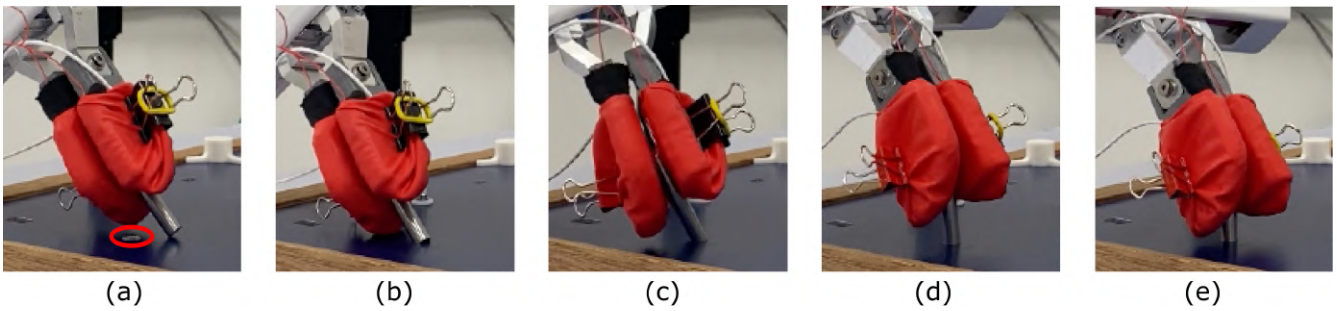

Fig. 7. Snapshots of a successful insertion. (a) The robot is exploring the taskboard. The red circle highlights the position of the hole. (b) The hole is found using tactile sensing measurements. (c) The robot moves to align the peg with the vertical to the plane, using the closed loop control described in Section V. (d) The remaining misalignment due to the coarse resolution of the tactile system is corrected by performing a spiral movement. (e) The peg falls into the hole.

TABLE I
SUMMARY OF THE 40 TRIALS STARTING FROM DIFFERENT INITIAL POSITIONS.

Stage	Success Rate	Average Time (s)
Search	39/40	19.9
Insertion	38/39	24.1
Adjustment	38/38	10.1

the target hole was successfully detected 39 times. The single failure was caused by a sudden change in the average taxel responses corresponding to a false detection of the hole (see Section IV). The insertion phase was successful 38/39 times, where the failure was due to a large error in the computation of the in-hand angle θ. It must be noted that the final open-loop adjustment was required for each attempt due to the error in the computation arising from the coarse resolution of the used sensor. The final spiral adjustment was triggered when $|\phi| < 15°$. The radius of the spiral increased linearly over 20 seconds up to a maximum of 0.025 m. During the experiments, we observed the angle θ to vary up to a maximum of 73° with respect to the initial grasping orientation. A sequence of images showing the robot executing the PiH task is given in Figure 7.

As visible from Table I the proposed method took an average of 54.1 s to complete the task. The search time depends on the size of the area of interest making it difficult to draw a comparison with other approaches. In general, the average time to successfully execute the task is larger compared to the works previously discussed where the peg was rigidly connected to the robot flange or firmly grasped. However, it must be noted that the difficulty of the task in terms of peg-hole clearance is comparable with the state of the art, but in our case we also considered the peg to be free to pivot in hand.

A possible solution to reduce the execution time would consist in increasing the control gains. This was not possible with the current setup. Indeed, this version of the tactile system can currently be sampled at 10 Hz. To increase the gains in these conditions would lead to jerky robot movements. Thus, generating high contact forces that can change the in-hand position of the peg, such that the assumption made in Section II does not hold. Moreover, high gains applied in these conditions can make the controller unstable.

VIII. CONCLUSION

In this paper, we address the PiH problem by proposing an insertion strategy driven by tactile feedback. Compared to the previous literature, the proposed method does not require the peg to be fixed to the robot end-effector and can handle in-hand rotation of the object, which is captured using the sense of touch. We tested our approach with a small peg-hole clearance, comparable to that used to benchmark the previously discussed methods, which assumed the peg was connected to the robot end-effector. In particular, the proposed approach achieved 38/40 successful insertions with a 0.1 mm clearance. Compensating for peg rotation increases the time required to complete the task. However, as previously discussed, we were mainly limited by the slow sampling frequency of the tactile measurements. In a future extension of the work, the use of other sensors providing faster sampling times will be investigated. Moreover, future developments of the approach will aim to generalise to different peg geometries, such as squared pegs, whilst using higher resolution sensors capable of also providing information on shear forces.

REFERENCES

[1] A. Fancello, J. Porter, and E. Reinhart, "Force reflection effects on operator performance of remote maintenance and inspection systems," in *Non-Destructive Testing*, J. Boogaard and G. van Dijk, Eds. Oxford: Elsevier, 1989, pp. 725–730.

[2] J. Jiang, Z. Huang, Z. Bi, X. Ma, and G. Yu, "State-of-the-art control strategies for robotic pih assembly," *Robotics and Computer-Integrated Manufacturing*, vol. 65, p. 101894, 2020. [Online]. Available: https://www.sciencedirect.com/science/article/pii/S0736584519302418

[3] J. Xu, Z. Hou, Z. Liu, and H. Qiao, "Compare contact model-based control and contact model-free learning: A survey of robotic peg-in-hole assembly strategies," *arXiv preprint arXiv:1904.05240*, 2019.

[4] L. Lin, Y. Yang, Y. Song, B. Nemec, A. Ude, J. Rytz, A. Buch, N. Krüger, and T. Savarimuthu, "Peg-in-hole assembly under uncertain pose estimation," in *Proceeding of the 11th World Congress on Intelligent Control and Automation*, 2014, pp. 2842–2847.

[5] "Peg-on-hole: a model based solution to peg and hole alignment," *Proceedings - IEEE International Conference on Robotics and Automation*, vol. 2, pp. 1919–1924, 1995.

[6] W. Newman, Y. Zhao, and Y.-H. Pao, "Interpretation of force and moment signals for compliant peg-in-hole assembly," in *Proceedings 2001 ICRA. IEEE International Conference on Robotics and Automation (Cat. No.01CH37164)*, vol. 1, 2001, pp. 571–576 vol.1.
[7] J. Oh and J.-H. Oh, "A modified perturbation/correlation method for force-guided assembly," *Journal of Mechanical Science and Technology*, vol. 29, 2001.
[8] H.-C. Song, Y.-L. Kim, and J.-B. Song, "Guidance algorithm for complex-shape peg-in-hole strategy based on geometrical information and force control," *Advanced Robotics*, vol. 30, no. 8, pp. 552–563, 2016. [Online]. Available: https://doi.org/10.1080/01691864.2015.1130172
[9] H. Qiao and S. Tso, "Three-step precise robotic peg-hole insertion operation with symmetric regular polyhedral objects," *International Journal of Production Research*, vol. 37, no. 15, pp. 3541–3563, 1999. [Online]. Available: https://doi.org/10.1080/002075499190176
[10] "Hole detection algorithm for chamferless square peg-in-hole based on shape recognition using f/t sensor," *International Journal of Precision Engineering and Manufacturing 2014 15:3*, vol. 15, pp. 425–432, 2014.
[11] "Intuitive peg-in-hole assembly strategy with a compliant manipulator," *2013 44th International Symposium on Robotics, ISR 2013*, 2013.
[12] "Compliance-based robotic peg-in-hole assembly strategy without force feedback," *IEEE Transactions on Industrial Electronics*, vol. 64, pp. 6299–6309, 8 2017.
[13] T. Zhang, X. Liang, and Y. Zou, "Robot peg-in-hole assembly based on contact force estimation compensated by convolutional neural network," *Control Engineering Practice*, vol. 120, p. 105012, 2022.
[14] S. Kim and A. Rodriguez, "Active extrinsic contact sensing: Application to general peg-in-hole insertion," 2021.
[15] "Comparative peg-in-hole testing of a force-based manipulation controlled robotic hand," *IEEE Transactions on Robotics*, vol. 34, pp. 542–549, 2018.
[16] J. Bimbo, S. Luo, K. Althoefer, and H. Liu, "In-hand object pose estimation using covariance-based tactile to geometry matching," *IEEE Robotics and Automation Letters*, vol. 1, no. 1, pp. 570–577, 2016.
[17] S. Dikhale, K. Patel, D. Dhingra, I. Naramura, A. Hayashi, S. Iba, and N. Jamali, "Visuotactile 6d pose estimation of an in-hand object using vision and tactile sensor data," *IEEE Robotics and Automation Letters*, vol. 7, no. 2, pp. 2148–2155, 2022.
[18] A. Albini, F. Grella, P. Maiolino, and G. Cannata, "Exploiting distributed tactile sensors to drive a robot arm through obstacles," *IEEE Robotics and Automation Letters*, vol. 6, pp. 4361–4368, 7 2021.
[19] D. Ma, S. Dong, and A. Rodriguez, "Extrinsic contact sensing with relative-motion tracking from distributed tactile measurements," in *2021 IEEE International Conference on Robotics and Automation (ICRA)*, 2021, pp. 11 262–11 268.
[20] "Pressure distribution classification and segmentation of human hands in contact with the robot body:," vol. 39, pp. 668–687, 3 2020. [Online]. Available: https://journals.sagepub.com/doi/full/10.1177/0278364920907688
[21] L. Rocha, L. Velho, and P. de Carvalho, "Image moments-based structuring and tracking of objects." 01 2002, pp. 99–105.
[22] S. R. Chhatpar and M. S. Branicky, "Search strategies for peg-in-hole assemblies with position uncertainty," *IEEE International Conference on Intelligent Robots and Systems*, vol. 3, pp. 1465–1470, 2001.
[23] "Nist taskboard," https://www.nist.gov/el/intelligent-systems-division-73500/robotic-grasping-and-manipulation-assembly/assembly.
[24] "Cyskin," https://www.cyskin.com/.